Original Research Article

IONOSPHERIC TOTAL ELECTRON CONTENT RESPONSE TO THE INTENSE GEOMAGNETIC STORM OF 10TH -11TH MAY 2024 OVER LOW, MID AND HIGH LATITUDE GNSS STATIONS

Abstract

In this paper, we investigated the response of ionospheric Total electron content (TEC) to the intense geomagnetic storm of 10th - 11th May 2024 using 6 Global Navigation Satellite System (GNSS) stations: BAKE (Geog. Lat.64.33º N; Geog. Lon. 96.02º W), BELE (Geog. Lat. 1.41º S; Geog. Lon. 48.46º W), MBAR (Geog. Lat. 0.60º S; Geog. Lon. 30.74º E), SUTH (Geog. Lat. 32.38º S; Geog. Lon. 20.81º E), BJFS (Geog. Lat. 39.61º N; Geo. Lon. 115.89º E) and DUND (Geog. Lat. 45.88º S; Geog. Lon.170.60º E) situated over low, mid and high latitude regions. The GPS-TEC data was extracted, processed and used to plot vertical total electron content (VTEC) verses universal time (UT) from 8th to 13th May 2024 for each GNSS receiver station. A contour plot of TEC variation was also plotted for each station from 8th to 13th May 2024. The results showed TEC enhancing significantly at the beginning of the storm, during daytime at the geomagnetic equator, with the exception of MBAR, where TEC increased at night. This was attributed to the effect of prompt penetration of electric field (PPEF). A reduction in TEC was also noted on 11th May 2024, during the recovery phase over all the GNSS receiver stations. This was attributed to the effect of the disturbance dynamo electric field (DDEF) and composition change. The contour plots showed diurnal variation in TEC concentration over each GNSS receiver station. The TEC concentration however reduced during the storm period.

Keywords: Geomagnetic storm, Total Electron Content, Prompt Penetration Electric Field, Disturbance Dynamo Electric Field, Global Navigation Satellite System.

1.0 Introduction

“Geomagnetic storms are disturbances of the Earth’s magnetic field as a result of perturbations in the interplanetary magnetic field (IMF)” [1]. On 10th May 2024, the National Oceanic and Atmospheric Administration (NOAA) scientists witnessed a severe (G4)

geomagnetic storm where several Earth-directed Coronal Mass Ejections (CMEs) were in transit towards the Earth's outer atmosphere. The primary source of this activity was believed to be a large sunspot of NOAA cluster 13664 (AR13664) whose diameter had grown to up to 17 times the diameter of the Earth. This storm was predicted to rival the intensity of the Carrington event of 1859 which set telegraph stations on fire and disrupted global communication systems. The most recent severe (G4) storm occurred on 23rd March 2024 while the Halloween storms which occurred in October 2003 marked the last extreme (G5) event. The 10th -11th May 2024 geomagnetic storm had a disturbance storm time (Dst) index of ~ -412 nT, which makes it the greatest storm in over two decades. A geomagnetic storm of such a magnitude has various potential effects on modern infrastructure which include degrading of Global Positioning satellite systems (GPS) for hours, blacked out radio propagation systems [2], orientation and tracking problems on space craft, voltage control problems in power grid [3,4] and surface charging and increased drag on Low Orbit Satellites (LOS) Despite the above mentioned potential risks, this storm also triggered magnificent nighttime auroras or Northern lights in as low as Florida and Texas in the Southern states and down to Southern California on the West Coast and Missouri in the Midwest. Studies by various researchers have shown that the occurrences of geomagnetic storms have a large influence on the electrodynamics of the Earth's ionosphere through drastic changes in the ionospheric density structures (ionospheric F-region electron densities) [5] and total electron content (TEC) [6]. TEC is defined as the total number of electrons in a column of 1m^2 between a GPS satellite and a GPS receiver (1 TECU = 10^{16} electrons/m^2) [7-11]. It is measured in total electron content units (TECU). It is a key parameter that has been used to depict the charge densities of various ionospheric layers [12-14]. "It is expressed as an integral of electron density along the ray path between the receiver and the satellite as follows,

$$TEC = \int_{l_1}^{l_2} n_e(l)dl \quad (1)$$

where l_1 and l_2 are the position of the receiver and the satellite respectively, $n_e(l)$ is the variable electron density along the path from the satellite to the receiver and dl is the change in the distance between the receiver and the satellite" [15].

TEC undergoes significant changes during geomagnetic storms as a result of an influx of energetic particles into the ionosphere by the solar wind. This leads to changes in ionospheric density structures of TEC. The increases in the ionospheric density structures and TEC are known as positive storm effects while their decreases are known as negative storm effects. The occurrence and magnitude of the positive and negative storm effects largely depends on

local time, latitude, the phase of the storm [16, 17] and the competing effects of prompt penetration electric fields (PPEF) and disturbance dynamo electric fields (DDEF) [18]. Rukundo, [19] "used a daily variation of TEC from GNSS stations, ionosonde parameters and modeled zonal and meridional wind velocities to investigate the ionospheric TEC response over the African region. The equatorial GNSS station of NKLG recorded initial positive storm effects around the time of sudden storm commencement (SSC), which spread over the whole African region during the main phase with positive and negative storm effects during the main and recovery phases respectively. The ionospheric response was due to the relative contributions of prompt penetration electric field effects and equatorward traveling disturbances which depended on storm onset time, past ionospheric state, and storm phase". Oikonomou et al [20] investigated the "negative ionospheric response over the European sector during two storms that took place on 8th September 2017, by exploiting observations over ten European locations. The spatial and temporal variations of TEC, foF2 and hmF2 ionospheric characteristics were examined so as to explain the physical mechanisms underlying the strong negative ionospheric response. They detected very sharp electron density (in terms of foF2 and TEC) decrease during the main phases of the two storms and attributed it to the large displacement of the Mid-latitude Ionospheric Trough (MIT). Their study also revealed that the two storms showed different features caused by different processes. Large Scale Traveling Ionospheric Disturbances (LSTIDs) were also observed during both storms, followed by enhanced Spread F conditions over Digisonde stations. The regional dependence of ionospheric storm effects was demonstrated by observing the behavior of ionospheric effects over the northern part of Europe being different from that over the southern part". Mishra et al., [21] studied "TEC during three intense geomagnetic storms of the year 2015: during 16 - 21 March 2015 (The St. Patrick's Day storm), 21 - 24 June 2015 and 18 - 22 December 2015. They observed that equatorial and low-latitude regions were largely affected by the geomagnetic storms. All these results suggested that the acute disruption of global winds (surging towards the equator from higher latitudes) and electric fields commenced from magnetosphere-ionosphere interaction cause the severe modification in the equatorial, low latitude region". Sharma et al., [22] investigated "the ionospheric response to a severe geomagnetic storm on St. Patrick's Day (17th March 2015) and a strong geomagnetic storm on 7th October 2015 over the low-latitude Saudi Arab region. The GNSS-TEC observations over low latitude RASH station (28◦29N, 34◦46E) in Saudi Arab confirmed that the spatial temporal alterations over the region not only depended on the low-latitude electrodynamics but also relied on the high and mid-latitude electrodynamics. During the St. Patrick's Day storm, the minimum Dst reached to -223 nT with AE

enhancement up to 2215 nT and VTEC values showed maximum enhancement of 250.16% with comparison to average quiet days VTEC (positive effect of geomagnetic storm). The positive response of the VTEC was also observed over the region due to the coexistence of PPEF with the prevailed long duration DDEF. The F2 layer got uplifted with the enhanced fountain effect through the equatorial E × B drift, which was observed with the enhancement in hmF2 and enhancement in O/N2 ratio. For the strong geomagnetic storm event of 7th October 2015, minimum Dst reached -124 nT with AE enhancement up to 1209.30 nT and VTEC values showed minimum decrement of -72.14% as compared to the average quiet days VTEC (negative effect of geomagnetic storm). The negative response of VTEC was observed during the main phase of the storm and was attributed to the consequences of suppressed EIA over the observatory station. The negative response was described by the downward movement of F2 layer with apparent reduction in hmF2 and depletion in O/N2 ratio over the low latitude region. The results during the storm period also showed that the intensity of amplitude scintillation was enhanced over the low latitude region whose magnitude depended on the severity of the geomagnetic storm". Singh & Sripathi, [23] studied the "ionospheric response of the equatorial and low-latitude ionosphere to the 22nd to 23rd June 2015 geomagnetic storm over India using ground based Ionosondes located at Tirunelveli (8.73°N, 77.70°E; geomagnetic latitude: 0.32°N), Hyderabad (17.36°N, 78.47°E; geomagnetic latitude: 8.76°N), and Allahabad (25.45°N, 81.85°E; geomagnetic latitude: 16.5°N) along with a chain of GPS receivers. The uniqueness of this storm was that in contrast to the equatorial plasma bubbles that were detected in the European sector, they observed suppression of plasma bubbles in the Indian sector. The observations suggested that westward penetration electric field during local midnight caused abrupt decrease of virtual height (h'F (km)) to ~200 km and suppressed plasma bubbles due to under-shielding. The layer later increased to 500 km simultaneously due to over-shielding effect. On 23rd June 2015, they observed negative storm effects in the Northern Hemisphere and positive storm effects in the Southern Hemisphere. The absence of equatorial Es layers at Tirunelveli and presence of F3 layer at Tirunelveli/Hyderabad seemed to be associated with equatorial electrojet (EEJ)/counter electrojet (CEJ) variations. On 24th June 2015, they observed strong negative storm effects at Allahabad/Hyderabad and positive storm effects at Tirunelveli. The enhancement of h'F (km) over all three Ionosonde stations at 20:30 UT on 23rd June 2015 during recovery phase suggested the presence of eastward DDEF that caused pre-sunrise spread F at Hyderabad/Allahabad. The void of spread F at Tirunelveli suggested its mid-latitude origin. Periodogram analysis of foF2 and h'F (km) in the present analysis suggested

the presence of shorter periods (~< 2 h) associated with PPEF while larger periods (>2 h) associated with DDEF".

In this paper, we study and present results on the ionospheric TEC response to the 10^{th} – 11^{th} May 2024 geomagnetic storm over 6 Global Navigation Satellite Systems (GNSS) receiver stations situated at the high, middle and low latitude regions. This storm was quite unique since it was accompanied by extreme solar flares and also produced aurorae at far more equatorial latitudes in both northern and southern hemispheres [24].

2.0 Materials and methods

2.1 Data sources

2.1.1 Geomagnetic indices and solar wind parameters data

In this study, the variations of Solar wind Parameters: Z-component of Interplanetary magnetic field (IMF-Bz), Y component of Interplanetary Electric Field (IEF-Ey), solar wind speed (SW Speed) , kp and Dst indices for 8^{th} – 13^{th} May 2024 were obtained from Omniweb website: *https://omniweb.gsfc.nasa.gov/form/dx1.html.*

2.1.2 Solar activity data

The solar activity between 1^{st} and 31^{st} May 2024 was obtained from the *NOAA* website: NOAA/*Spaceweatherlive.com.*

2.1.3 GPS data

In this study, the GPS-TEC data over 6 stations: BAKE, DUND, BELE, MBAR, BJFS and SUTH in Figure 1 were accessed from the University of NAVSTAR Consortium website: *http:/gage-data.earthscope.org/archive/gnss/rinex.*

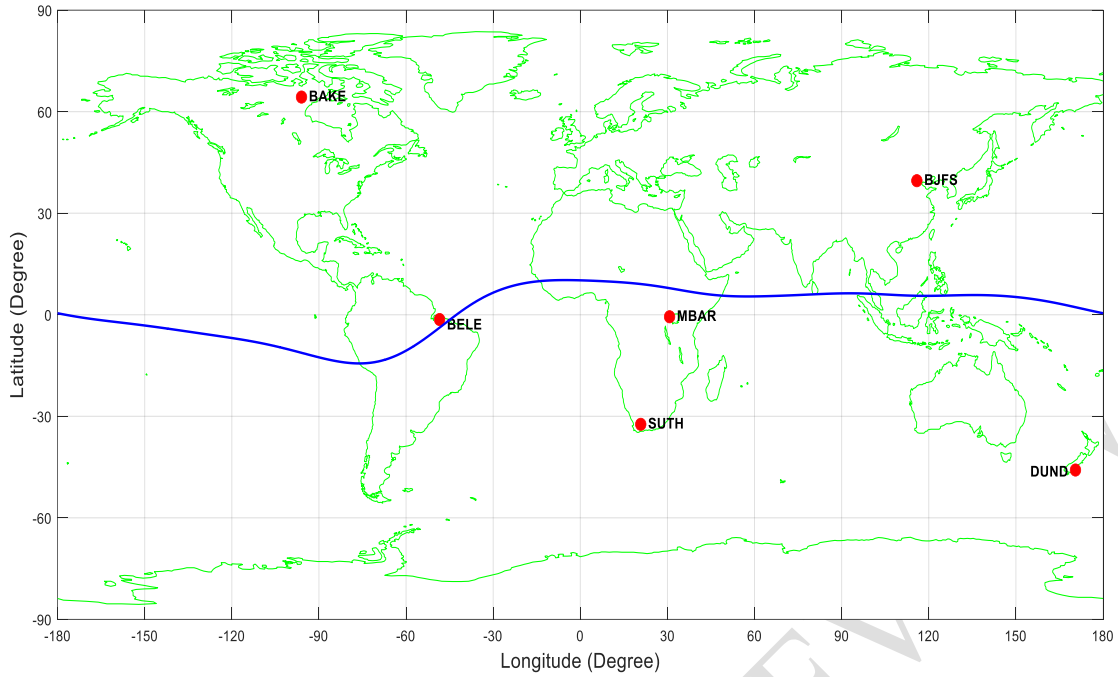

Figure 1: Map showing geographical locations of BAKE, BELE, MBAR, SUTH, BJFS and DUND GNSS receiver stations.

2.2 Methodology

2.2.1 Processing TEC data

TEC data in the GNSS receivers is saved in the zipped Receiver Independent Exchange (RINEX) format. The RINEX files are converted to observable files with the use of Gopi software [25, 26]. The GNSS measurements in this case are either code pseudoranges (P) or carrier phases (ϕ). The GNSS receiver receives the code time delay and carrier phase difference by cross-correlating the f_1 and f_2 modulated carrier signals, which are normally considered to travel along the same path through the ionosphere [27]. The estimates of GNSS-derived ionospheric TEC are obtained using dual frequency GNSS measurements [28, 29]. The GNSS data from the receiver are critical for estimating the electron density along a ray path between a satellite and a ground receiver [30, 31]. Dual-frequency GPS receivers may offer integral information on the ionosphere and plasmasphere by computing the differential of the code and carrier phase measurements, and also removing ionospheric inaccuracies in TEC estimates [32, 33] As a result, the TEC computed by the dual-frequency receivers is offered as an input to an ionosphere assimilation model [34]. For the present study, GNSS data collected in dual-frequency receivers was used, and TEC data was obtained using the pseudo-range and carrier phase measurements. The TEC calculated from the pseudo-range measurement (slant TEC) is given by Equation 2:

$$STEC = \frac{1}{40.3}\left[\frac{f_1^2 f_2^2}{f_1^2 - f_2^2}\right](P_2 - P_1) \quad (2)$$

Similarly, the TEC from carrier phase measurement is calculated as follows using Equation 3:

$$STEC = \frac{1}{40.3}\left[\frac{f_1^2 f_2^2}{f_1^2 - f_2^2}\right](\phi_2 - \phi_1) \quad (3)$$

where f_1 and f_2 are GPS satellite frequencies determined from the fundamental frequency, f_o =10.23MHz as: (f_1=154, f_o=1,575.42MHz, (f_2=120, f_o=1,227.60 MHz), and the differential code and phase measurements are ($P_2 - P_1$) and ($\phi_1 - \phi_2$), respectively [35].

Figure 2 shows the geometry for converting STEC to VTEC.

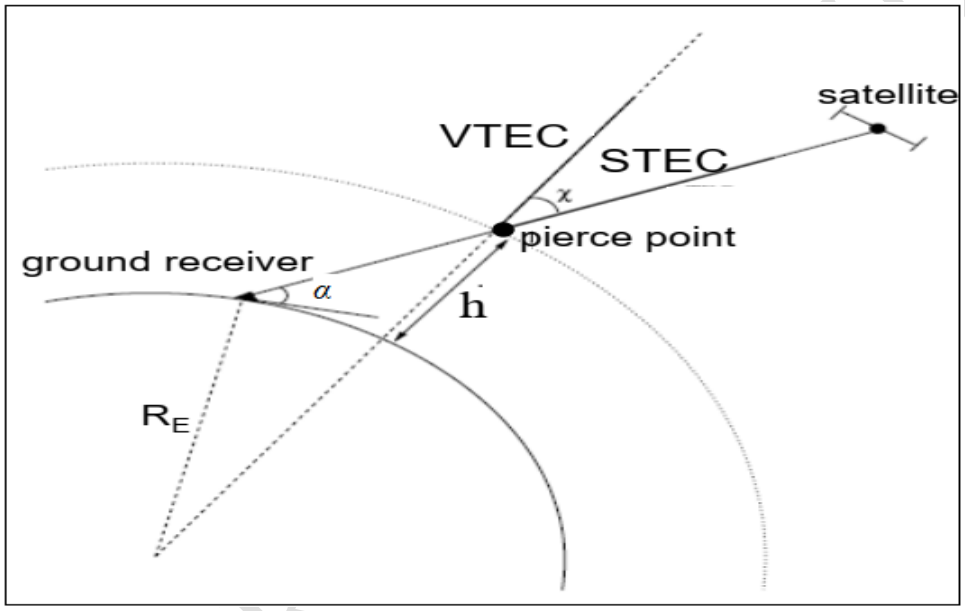

Figure 2: Geometry for converting slant TEC and vertical TEC

The vertical total electron content (VTEC) is obtained using Equation 4:

$$VTEC = STEC \times Cos(\chi') \quad (4)$$

where the zenith angle χ' is given by Equation 5:

$$\chi' = \arcsin\left[\frac{R_E \cos\alpha}{R_E + h} Sin(\chi)\right] \quad (5)$$

VTEC is therefore given by equation 6:

$$VTEC = STEC\left\{\cos\left[\arcsin\left(\frac{R_E \cos\alpha}{R_E + h}\right)\sin(\chi)\right]\right\} \quad (6)$$

Where α is the satellite's elevation angle, R_E is the Earth's mean radius and is considered to be approximately 6371 km, and h is the height of the ionospheric layer, which is considered to be 400 km [36 - 38].

The average daily data of VTEC for all PRNs for each selected day and GNSS receiver station were obtained by averaging VTEC values for all identical pseudo-random numbers (PRNs) within a 24 hour period [39]. The data was then used to plot VTEC against Universal Time (UT) for each day from 8th to 13th May 2024 and for each GPS receiver station as indicated in Figure 5-10. The VTEC against UT plots for each day were analyzed.

To comprehend how the geomagnetic storm affected ionospheric TEC changes on a range of scales in low, middle and high latitude regions, we employed contour plot of TEC variation for each GNSS receiver station as indicated in Figure 11.

Information for the 6 GNSS receiver stations: BAKE, DUND, SUTH, BELE, MBAR and BJFS were used in this study is given in Table 1:

Table 1: Geographic locations of BAKE, DUND, SUTH, BELE, MBAR and BJFS

STATION ID	COUNTRY	REGION	GEOG. LAT	GEOG. LON	LOCAL TIME (LT)
BAKE	Canada	High latitude	64.33ºN	96.02ºW	LT=UT – 6
DUND	New Zealand	Mid- Latitude	45.88ºS	170.60ºE	LT=UT + 11
SUTH	South Africa	Mid-latitude	32.38ºS	20.81ºE	LT=UT + 1
BJFS	China	Mid-latitude	39.61ºN	115.89ºE	LT=UT + 8
BELE	Brazil	Low-latitude	1.41ºS	48.46ºW	LT=UT – 3
MBAR	Uganda	Low-latitude	0.60ºS	30.74ºE	LT=UT + 2

3.0 Results

3.1. The variation of IMF-Bz, IEF-Ey, SW Speed, kp and Dst indices between 8th -13th May 2024

The variation of IMF-Bz, IEF-Ey, SW Speed, kp and Dst indices between 8th- 13th May 2024 were presented using as in Figure 3.

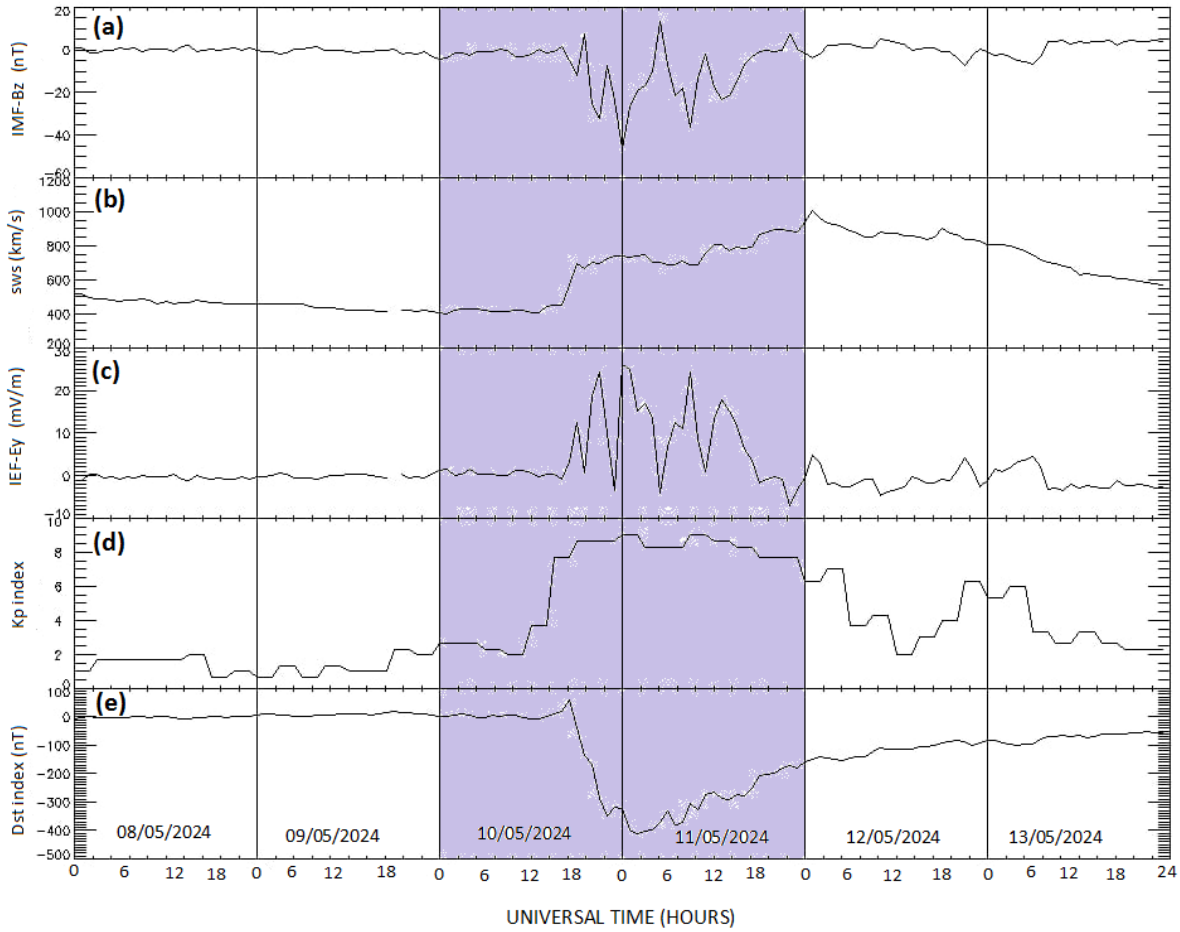

Figure 3: Plot of (a) IMF-Bz (b) SW speed (c) IEF-Ey (d) kp index (e) Dst index for 8th–13th May 2024 (*https://omniweb.gsfc.nasa.gov/form/dx1.html, accessed on 26th June 2024*)

In Figure 3(e), it is noted that the Geomagnetic storm began at about 18:00 UT on 10th May with a sudden commencement which was immediately followed by an initial stage. An increase in solar wind speed was also observed as in Figure 3(c). According to [40], the sudden storm commencement is due to the increase in the solar wind dynamic pressure. The main phase of the storm which is the defining phase of the storm occurred from 18:00 UT on 10th May 2024 to 03:00 UT on 11th May 2024. The main phase which reached its peak with a Dst of ~-412 nT at 03:00 UT, where IMF-Bz value was -45nT (Figure 3(a)) with a corresponding solar wind speed of 750km/h. The main phase represents the injection of the ring current resulting from the southward turning of the Interplanetary Magnetic Field (IMF-Bz) of -50.06 nT. The recovery phase which is associated with loss of ring current ions resulting from charge exchange with the neutral exosphere began at 03:00 UT on 11th May and progressed up to 15th May 2024. From Figure 3(e), it is noted that the 10th to 11th May 2024 was an ideal geomagnetic storm since it had all the four phases. The geomagnetic storm was classified as an intense storm since the Z-component of the interplanetary magnetic field (IMF) turned southward reaching to as much as -50nT and a solar wind reaching up to

1000km/s between 11th and 12th May 2024. Figures 3(c) showed that 8th and 9th May exhibited Kp Index values below 2. The kp index exhibited a rise in kp values between 12:00 and 24:00 UT on 10th May 2024 where it rose from 3 and reached a maximum value of 9 at 24:00 UT. The kp values remained above 6 for the whole day before dropping to kp values below 4 between 06:00 and 18:00 UT and rising steadily, reaching a maximum kp value of ~ 6.3. The Kp index of 9 during the 10th and 11th May 2024 clearly shows that it was an intense storm [41].

3.2. The variation of solar activity for May 2024

Figure 4 shows the number of C, M and X – class solar flares produced in May 2024 and its corresponding sunspot numbers. The plot brings out the solar activity during the month of May 2024. The solar wind and sporadic interplanetary disturbances such as shock waves, CMEs and solar flares are strongly affected by changes in solar activity [42].

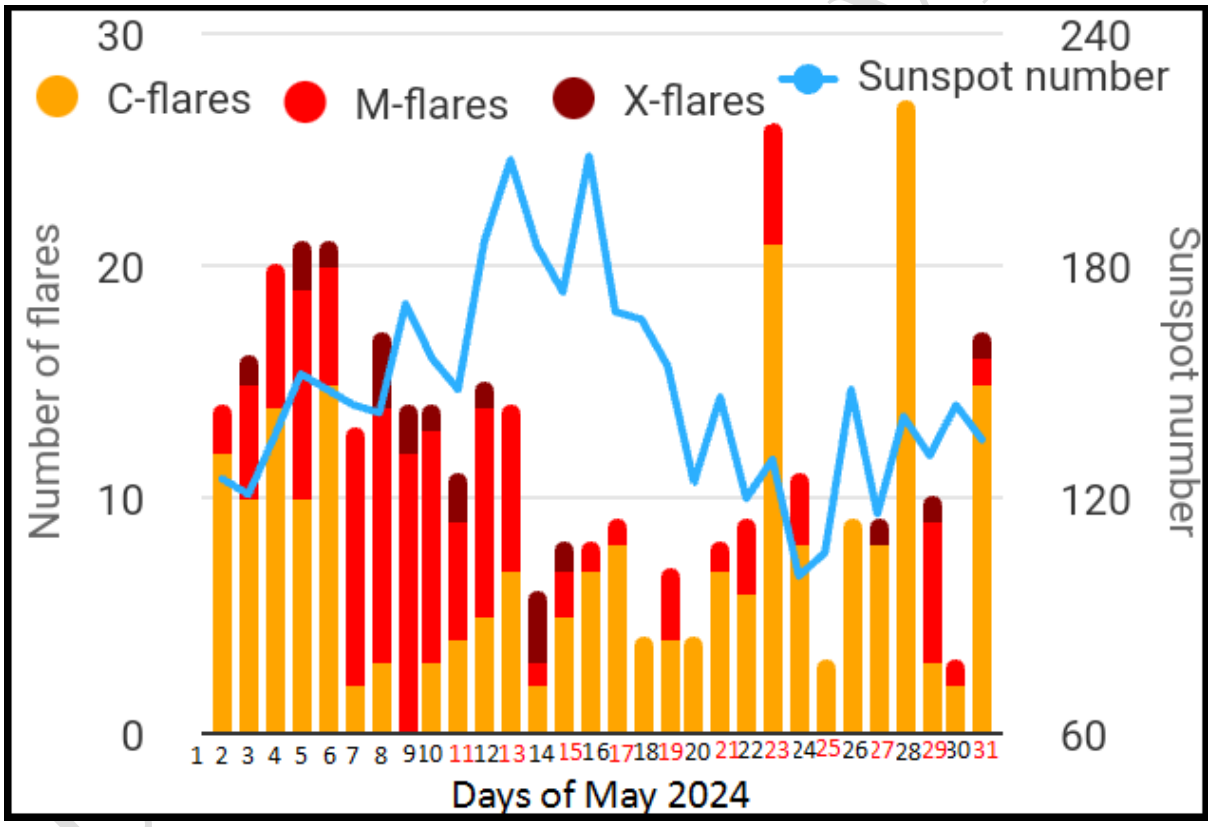

Figure 4: Variation of solar activity between 1st and 31st May 2024 (*NOAA/Spaceweatherlive.com, accessed on 1st June 2024*)

In Figure 4, the solar activity was observed to ramp up from 9th May 2024 reaching its maximum on 13th May 2024. This was depicted by the increase in sunspot numbers from ~ 140 to ~ 240. According to NOAA/spaceweatherlive.com, the M and X-class solar flares were seen to dominate between 8th and 13th May 2024. On 8th May 2024, the Sun's active

region of NOAA region number 13664 (AR13664) produced multiple M-class and a X1.0-class solar flares leading to the launching of Coronal Mass Ejections (CMEs) towards the Earth. On 9th May 2024, the AR13664 produced X2.25 and X1.12-class solar flares. These solar flares were associated with full-halo CMEs. On 10th May 2024, during the commencement of the storm, the AR13664 produced a X3.98-class solar flare. On 11th May 2024, the AR13664 produced a X5.7-class solar flare which was associated with another asymmetrical full-halo CME. The NOAA space weather prediction center observed that the AR13664 also caused an S1 solar radiation storm which rose up to S2. Solar flares leads to an increase in the ionization density in the ionosphere [43]. They largely affect the sub-solar and low latitude regions [44, 45]. It is noted in Figure 4 that there was a slight drop in sunspot numbers from 8th to 11th May 2024 before a steady rise from 11th to 13th May 2024.

3.3. The variation of the TEC over BAKE, DUND, SUTH, BJFS; BELE and MBAR on 8th, 9th, 10th, 11th, 12th and 13th May 2024

Figures 5-10 shows the variation of VTEC against universal time (UT) over BAKE, DUND, SUTH, BJFS, BELE and MBAR on 8th , 9th , 10th, 11th, 12th and 13th May 2024.

3.3.1. Variation of TEC against Universal time (UT) over BAKE

The variation of TEC against UT over BAKE is shown by Figure 5. On 8th May 2024, the GNSS receiver station, showed a gradual decrease in TEC from 00:00UT to 06:00UT, before rising gradually, reaching maximum TEC of 20 TECU at 22:00UT before dropping drastically up to 24:00 UT as indicated in Figure 5(a). On 9th May 2024, the TEC values over the GNSS receiver station dropped drastically to about 3 TECU between 06:00 and 08:00UT. The TEC values however began to rise, with attaining maximum TEC value of 17 at 22:00 UT. The TEC values were seen to decrease up to 24:00 UT as indicated in Figure 5(b). Figure 5(c) shows TEC variation on 10th May 2024. Here, the TEC values over the GNSS receiver station fluctuated by about 12 TECU at 05:00 UT, before rising up to 18:00 UT where it attained maximum values of about 20 TECU. It should be noted that this is the time the storm commenced. Large TEC fluctuations were observed from 18:00 UT on 10th May to about 03:00 UT on 11th May, which was the main phase of the storm. From 03:00 UT, the TEC values for the two GNSS receiver began to rise accompanied by small TEC perturbations as indicated by Figure 5(d). The rise in TEC corresponded well with the recovery phase of the storm phase. In Figure 5(e) 12th May 2024, the GNSS receiver station exhibited the same behavior of TEC like the one observed on 8th and 9th in Figure 5(a) and 5(b).

It is noted in Figure 5(c) and 5(d) that during the main phase, TEC over the GNSS receiver station exhibited positive storm effects while the recovery phase exhibited negative storm effects. TEC perturbations were observed during the storm period. The initial stage of the storm exhibited the highest TEC value (30 TECU) for the 6 days studied.

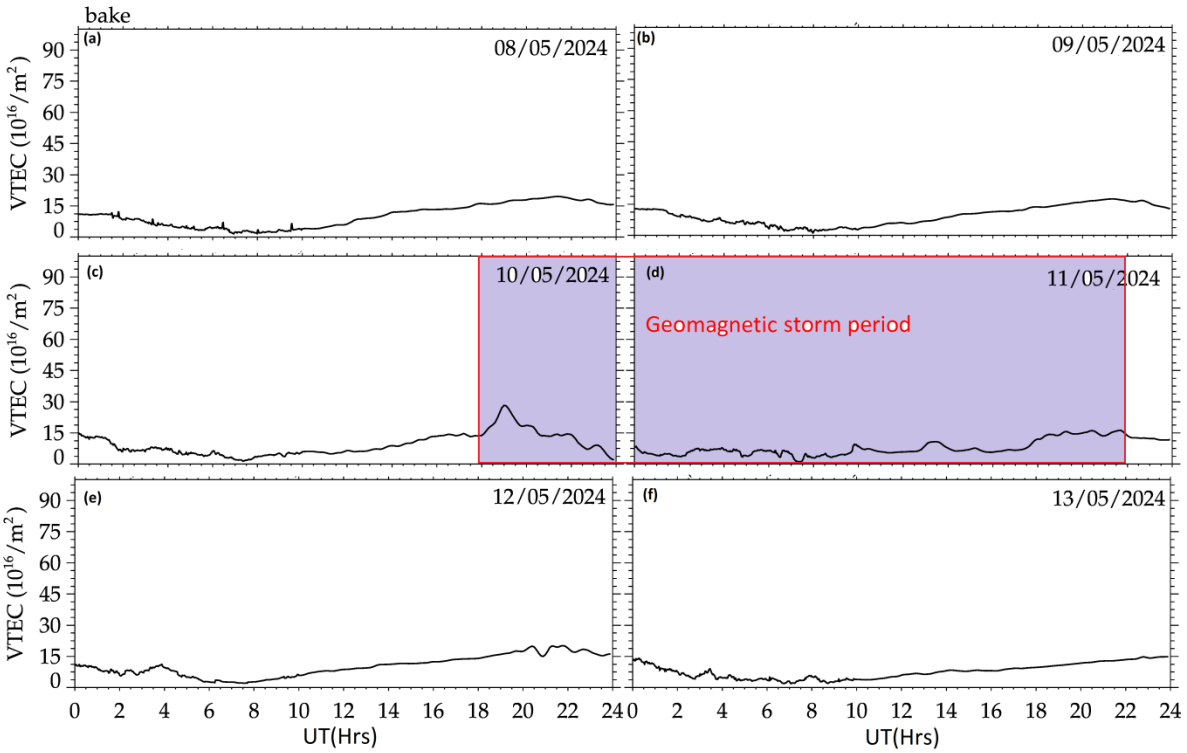

Figure 5: Plots of VTEC against UT over BAKE for: (a)08.05.2024 (b)09.05.2024 (c)10.05.2024 (d)11.05.2024 (e)12.05.2024 and (f)13.05.2024

3.3.2. Variation of TEC over DUND

The variation of TEC against UT over DUND is shown by Figure 6. On 8th and 9th May 2024, the GNSS receiver station, showed a gradual increase in TEC from 00:00UT to 04:00UT where it attained maximum TEC of 27 TECU, before dropping gradually, reaching a minimum TEC of 2 TECU at 19:00UT, before rising again up to 24:00 UT as indicated in Figure 6(a) and 6(b). On 10th May 2024, the TEC values rose from 00:00 to 04:00 UT before dropping drastically up to 10:00 UT. TEC fluctuations were observed between 10:00 and 18:00 UT. However, TEC began to rise from 18:00 UT on 10th May 2024, attaining a maximum TEC value of 36 TECU at 03:00 UT on 11th May 2024 as indicated in Figure 6(c) and 6(d). This rise in TEC corresponded well with the main phase of the storm. From 03:00 UT on 11th May 2024, the TEC values began fluctuating with increased perturbations up to

about 18:00 UT. This TEC fluctuation also corresponded well with the recovery phase of the storm.

Figure 6(e) and 6(f) showed TEC rising steadily from 00:00 UT to 03:00 UT, attaining a maximum TEC value of 40 TECU before dropping steadily, reaching its minimum at 18:00 UT. From 19:00 UT, the TEC value and reached its maximum TEC value of 40 TECU.

It is noted in Figure 6(c) and 6(d) that during the main phase, TEC over the DUND exhibited a negative storm effect while the recovery phase exhibited a positive storm effect. The peak of the storm exhibited the high TEC values. However the TEC value was lower than the one attained on 13th May 2024 for the same station. TEC perturbations were observed during the storm period as shown by Figure 6(c) and 6(d).

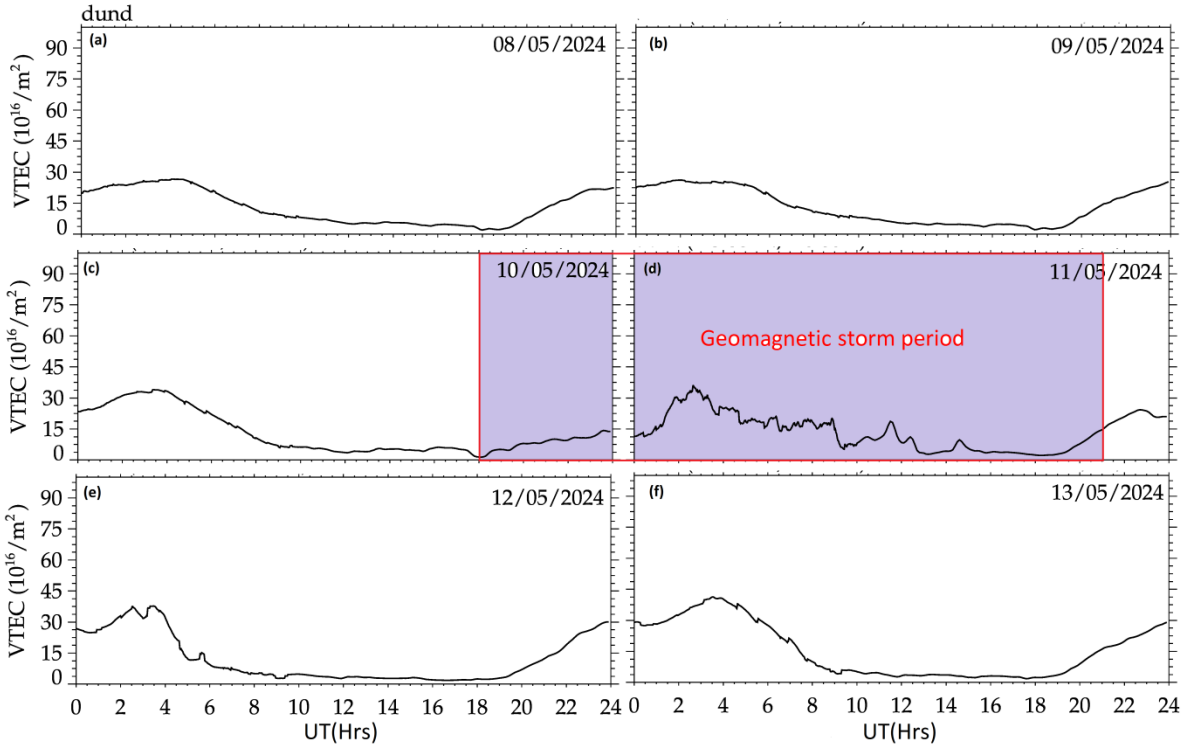

Figure 6: Plots of VTEC against UT over DUND for: (a)08.05.2024 (b)09.05.2024 (c)10.05.2024 (d)11.05.2024 (e)12.05.2024 and (f)13.05.2024

3.3.3. Variation of TEC over SUTH and BJFS

The variation of TEC against UT over SUTH is shown by Figure 7. On 8th and 9th May 2024, SUTH exhibited constant TEC of 4 TECU from 00:00UT to 05:00UT, before it began rising gradually, reaching maximum TEC of 47 TECU at 13:00UT. TEC values then dropped drastically up to 18:00 UT where it remained constant at 4 TECU for the rest of the day as indicated in Figure 7(a) and 7(b). On 10th May 2024, SUTH exhibited constant TEC of 4 TECU from 00:00UT to 05:00UT, before it began rising gradually, reaching maximum TEC

of 48 TECU at 13:00UT. TEC values then dropped drastically up to 18:00 UT when it began rising again and reached a maximum of 38 TECU on 14:00 UT on 11th May 2024 as indicated in Figure 7(c) and 7(d). Small TEC perturbations were also exhibited during the storm period. In Figure 7(e) and 7(f), 12th and 13th May 2024 exhibited a similar trend where TEC remained constant at 3 TECU from 00:00 to 04:00 UT, before it increased steadily up to 12:00 UT where it attained maximum TEC of 45 TECU on 12th and 52 TECU on 13th TECU. After 12:00 UT, both days exhibited a steady drop in TEC up to 18:00 when it remained constant at 3 TECU up to 24:00 UT

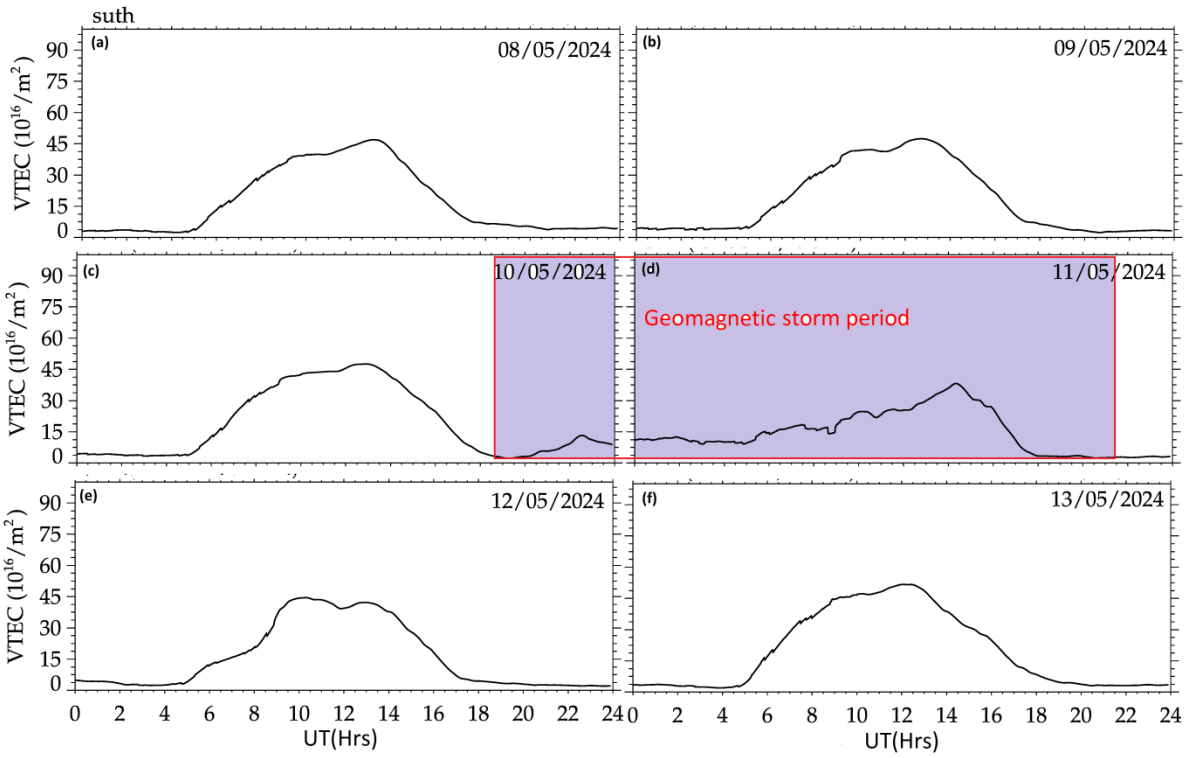

Figure 7: Plots of VTEC against UT over SUTH for: (a)08.05.2024 (b)09.05.2024 (c)10.05.2024 (d)11.05.2024 (e)12.05.2024 and (f)13.05.2024

The variation of TEC against UT over BJFS which is situated in the mid-latitude is shown by Figures 8. On 8th and 9th May 2024, BJFS exhibited a steady rise in TEC from 00:00UT reaching maximum TEC of 30 TECU at 05:00UT. TEC values then dropped drastically up to 0 TECU at 20:00 UT, before rising again and attaining a maximum TEC value of 20 TECU at 24:00 UT. On 10th May 2024, BJFS exhibited a steady rise in TEC, reaching maximum TEC of 35 TECU at 04:00UT. TEC values then dropped drastically up to 18:00 UT when it began rising again and reached a maximum of 28 TECU on 10:00 UT on 11th May 2024 as indicated in Figure 8(c) and 8(d). TEC perturbations were also exhibited during the storm period. In Figure 8(e) very low TEC values were exhibited during the whole day. In Figure 8(f), there was a steady rise TEC from 00:00 UT, reaching maximum TEC of 30 TECU at

06:00UT. TEC then dropped up to 20:00 UT before rising again and attaining a maximum value of 30 TEC at 24:00 UT.

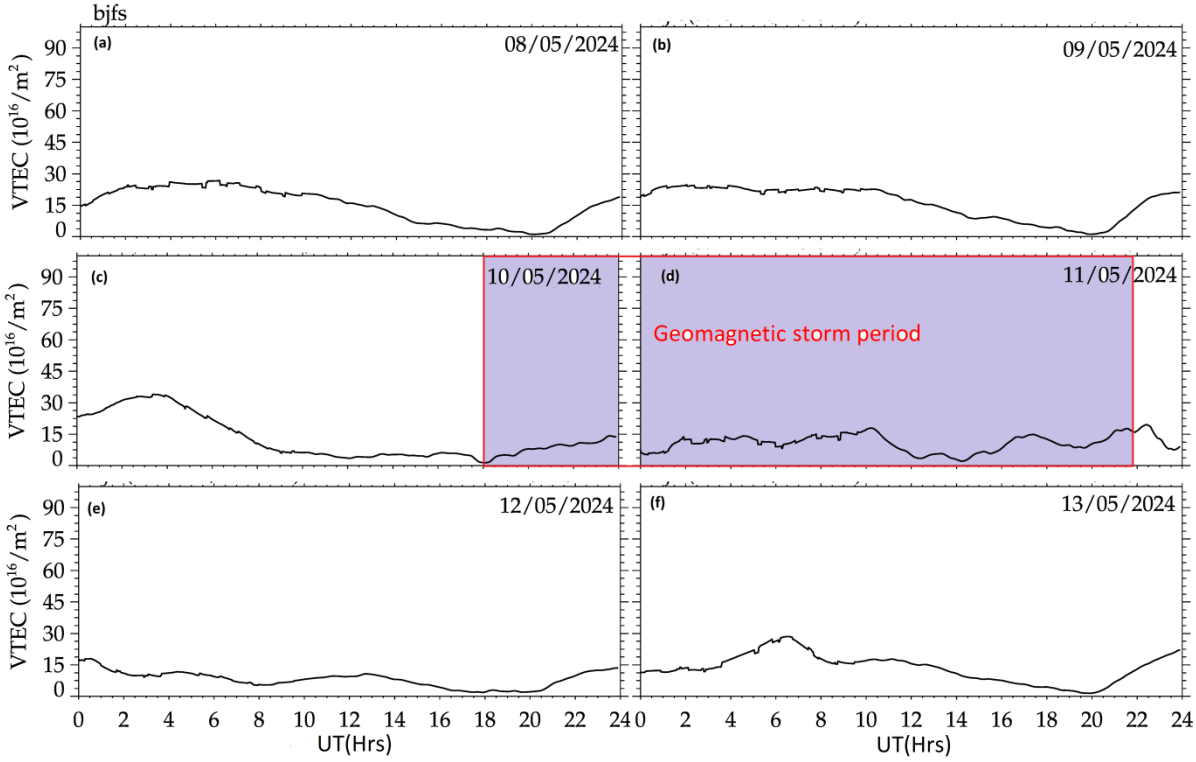

Figure 8: Plots of VTEC against UT over BJFS for: (a)08.05.2024 (b)09.05.2024 (c)10.05.2024 (d)11.05.2024 (e)12.05.2024 and (f)13.05.2024

3.3.4. Variation of TEC over BELE and MBAR

The variation of TEC against UT over BELE and MBAR are shown by Figures 9 and 10 respectively. In Figure 9(a) and 9(b), TEC exhibited a similar trend on 8th and 9th May 2024 over BELE. This was noted by both days having a decrease in TEC from 00:00 to 08:00 UT before rising steadily and attaining maximum TEC values of 70 TECU at 18:00 UT. It then dropped and attained a TEC value of 10 TEC at 24:00 UT. In Figure 10(a) and 10(b), TEC exhibited a similar trend over MBAR too. This was noted by both days having a decrease in TEC from 00:00 to 04:00 UT before rising steadily and attaining maximum TEC value of 78 TECU at 12:00 UT. On 10th and 11th May 2024, the TEC values over BELE and MBAR dropped slightly before rising steadily, reaching maximum TEC values of 78 TEC before dropping again. TEC depletions of depth 8 TEC followed by TEC enhancements were observed before the beginning of the main phase of the storm as indicated in Figure 9(c) and 10(c). There was a reduction in TEC over the two GNSS receiver stations during the main phase of the storm which was followed by an increase in TEC combined with perturbations during the recovery phase on 13th May 2024 as indicated in in Figure 9(d) and 10(d).

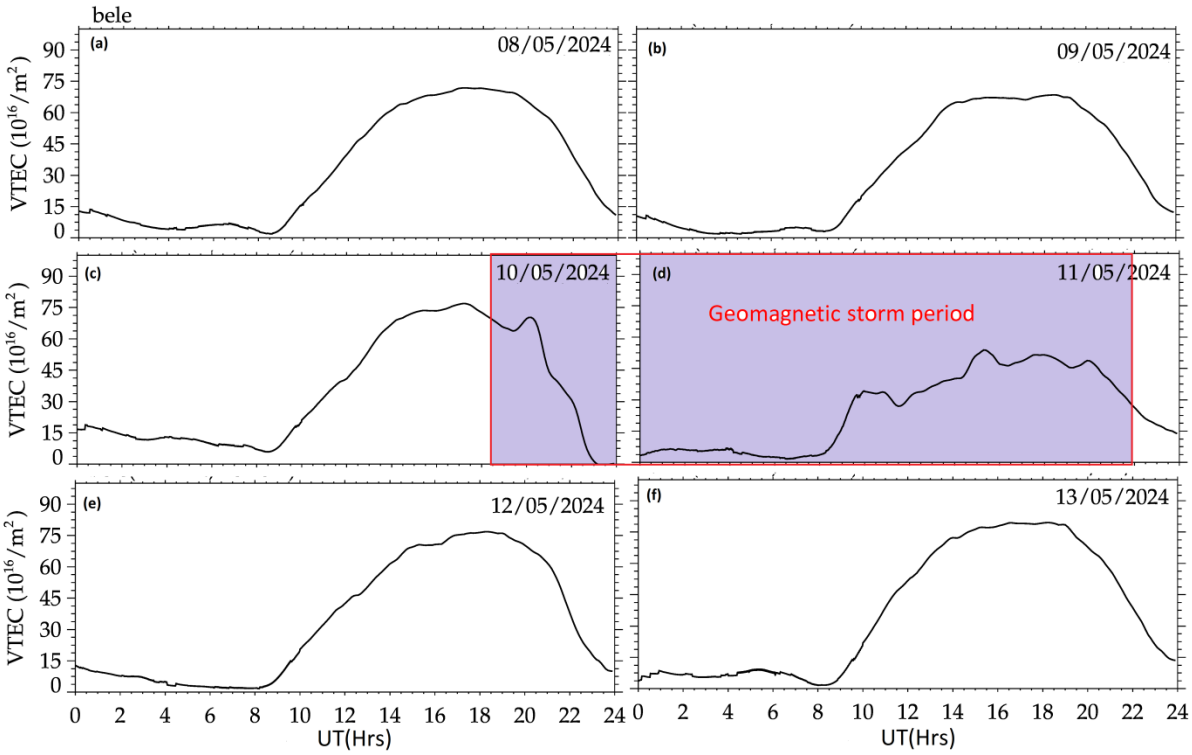

Figure 9: Plots of VTEC against UT over BELE for: (a)08.05.2024 (b)09.05.2024 (c)10.05.2024 (d)11.05.2024 (e)12.05.2024 and (f)13.05.2024

In Figure 10(e) and 10(f), TEC exhibited a steady rise from 03:00 UT, reaching maximum of 100 TECU on 12th May and 85 TECU on 13th May 2024 at 12:00 UT. A decline in TEC was noted from 12:00 UT to 18:00 UT where TEC depletions of about 15 TECU and 5 TECU were noted on 12th and 13th respectively, followed by TEC enhancements.

In Figures 9 and 10, it is noted that there were notable TEC depletions followed by TEC enhancement just before the commencement of the storm. TEC was seen to drop during the main phase of the storm. TEC over BELE and MBAR exhibited a positive storm effect during the main phase while the recovery phase exhibited a negative storm effect.

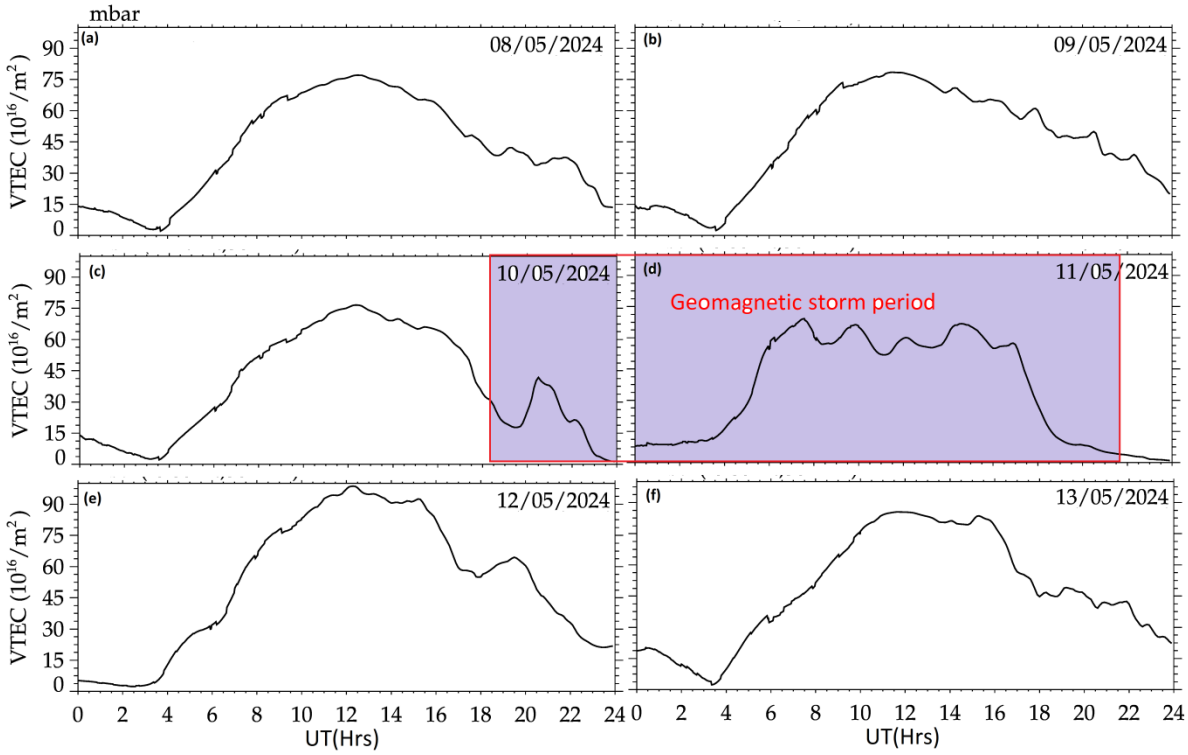

Figure 10: Plots of VTEC against UT over MBAR for: (a)08.05.2024 (b)09.05.2024 (c)10.05.2024 (d)11.05.2024 (e)12.05.2024 and (f)13.05.2024

3.4. Contour plots of TEC variations between 8th and 13th May 2024 over BAKE, DUND, SUTH, BELE, BJFS and MBAR

Figure 11 shows contour plots of TEC variations between 8th and 13th May 2024 over BAKE, DUND, SUTH, BJFS, MBAR and BELE. In Figure 11(a), BAKE had a TEC concentration of up to 20 TECU. However the TEC concentration reduced to values below 10 TECU during the storm. DUND had a TEC concentration of up to 30 TECU as shown in Figure 11(b). The TEC concentrations however reduced to between 20 and 25 TECU during the storm period. SUTH had TEC concentrations of up to 70 TECU as shown in Figure 11(c). During the storm, the TEC concentration reduced to 35 – 50 TECU. BJFS had a TEC concentration of up to 30 TECU as indicated by Figure 11(d). However, the TEC concentration dropped to between 0 and 30 TECU during the storm. At MBAR, TEC concentration reached a highest value of 70 TECU as indicated by Figure 11(e). However, the TEC concentration reduced to between 40 and 50 TECU during the storm period. BELE had a TEC concentration of up to 70 TECU as shown by Figure 11(f). However TEC concentration dropped to between 35 and 45 TECU.

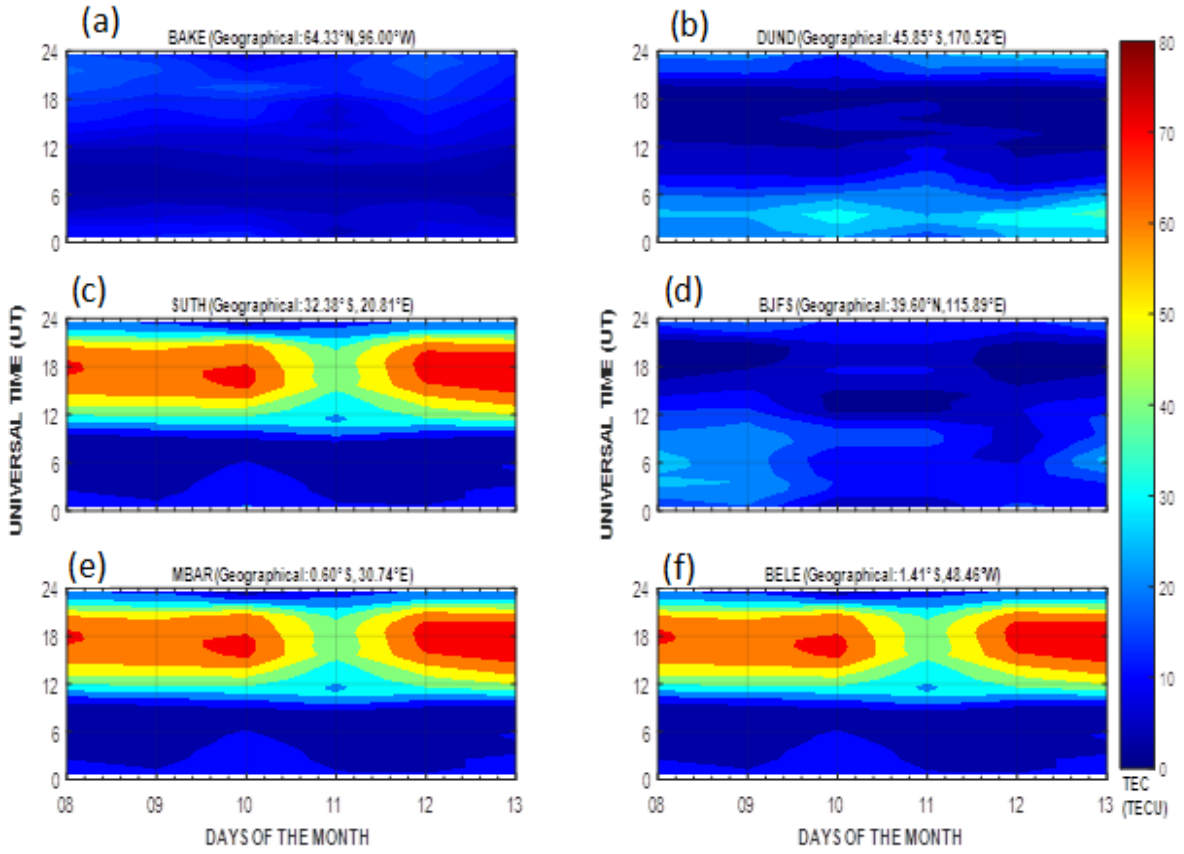

Figure 11: Contour plots of TEC variations for: (a) BAKE (b) DUND (c) SUTH (d) BJFS (e) MBAR (f) BELE

4.0 Discussions

The geomagnetic storm of 10th -11th May 2024 began on 10th May 2024 at 18:00 UT. An increase in VTEC was observed at BAKE and BELE (Figures 5(c) and 9(c)), which were on the dayside at the beginning of the storm (LT = 11:00 for BAKE, and LT=14:00 for BELE), and no change in VTEC at the other stations, which were on the nightside (LT=01:00 at BJFS, LT=04:00 at DUND, LT= 18:00 at SUTH) except the equatorial station: MBAR (LT=19:00), where an increase in TEC was observed despite the nightside at the beginning of the storm. These observations highlight the importance of the latitude and the local time of the location when the storm starts [46, 47]. The local time dependence of geomagnetic storms has been investigated by [48] using numerical simulation. According to the authors, the excessive heating of the thermosphere at high latitudes during magnetic storms drives global wind surge in the polar region. This wind then propagates to low latitudes with a bias for the night sector and dependence on the universal start time of the magnetic storm. Additionally, TEC was found to decrease during the recovery phase for all GNSS receiver stations as a result of composition change and movement [49-52] during the day, according to their

simulation. A few hours (around 19:30 UT) after the shock, during the main phase, it was observed that the geomagnetic storm caused a positive increase in VTEC at the equatorial stations: MBAR and BELE, respectively. This can be associated with the signature of PPEF. A study by Klimenko & Klimenko, [53] on the DDEF, PPEF and overshielding in the Earth's ionosphere during geomagnetic storm showed that the PPEF dominates at the early stages of geomagnetic storm during daytime. A decrease in TEC was observed in almost all stations the day following the geomagnetic storm. This was attributed to the DDEF signature [18]. In fact, PPEF and DDEF disturbances on the low-latitude ionosphere can result from geomagnetic storms, changing the variations in TEC across low-latitudes. During the day, the PPEF that arises during the main phase of a geomagnetic storm when the IM-Bz is moving southward enhances the eastward field and the E x B plasma drift at the equator [54-58]. The DDEF arising during recovery phase of storm when IMF-Bz is turned northward from its southerly course, is westward during the day and eastward during the night. Meridional winds can change during a geomagnetic storm and impact on the low-latitude TEC changes. In addition, positive as well as negative ionospheric storms (through global compositional changes) can also contribute to TEC variations at low-latitudes [19]. According to Singh et al., [46], the daytime eastward dawn-to-dusk prompt penetration electric field (PPEF) results in EXB plasma drift at equatorial latitudes during a positive geomagnetic storm. The upward E×B drift increases, results in increases in maximum height of F region and TEC that can last for several hours. Moreover, an impulsive energy deposition at high latitudes drives equatorward meridional winds and generates traveling atmospheric disturbances. These meridional winds have been shown to drag the ionospheric plasma to higher altitudes to the region where loss rates are lower, resulting in density enhancement.

It is important to note that the daytime electric field at the equator is eastward. This field, in conjunction with the Earth's magnetic field which is horizontal at the equator, gives rise to the vertical E×B drift of the ionospheric plasma. During magnetic storms, Joule energy dissipation in the auroral zone generates perturbations of thermospheric winds that, in turn, generate disturbed ionospheric electric fields and currents [59]. These disturbances propagate from the auroral zone toward low latitudes in few hours [60]. According to Fejer et al. [61] at the equator, an upward/downward vertical drift corresponds to an eastward/westward electric field. The effect of the PPEF process depends on the local time sector. This process produces an eastward electric field in the afternoon and evening and a westward electric field in the morning sectors. PPEF often produces an eastward/westward electric field during the day/night [62, 63]. The electric field in turn can enhance/reduce the E×B plasma drift in the dayside/nightside, thus increasing/decreasing TEC.

5.0 Conclusion

We have studied and presented results on the ionospheric TEC response to the intense geomagnetic storm of 10th – 11th May 2024 over six GNSS receiver stations situated over low, mid and high latitude regions. The results showed an increase in VTEC at the daytime stations. A positive TEC variation was observed at the equatorial MBAR station even though it was during the nighttime period. A decrease in TEC was observed at practically all GNSS receiver stations on 11th May, during the recovery phase of the storm. This was attributed to the composition change and movement during the day according to their simulation. During the main phase, the geomagnetic storm caused a positive increase in VTEC at the equatorial stations: MBAR and BELE. This was attributed to the effect of PPEF. This study revealed a difference in the response according to the local time during this storm. A particular TEC enhancement appeared at an equatorial station, MBAR which was on night side.

Data and materials availability

All data sets and software associated with this research are available and be obtained from the corresponding author on request

Disclaimer (Artificial intelligence)

Author(s) hereby declare that NO generative AI technologies such as Large Language Models (ChatGPT, COPILOT, etc.) and text-to-image generators have been used during the writing or editing of this manuscript.

Authors' contributions

This work was carried out in collaboration among all authors. All authors read and approved the final manuscript.

References

[1]Pokharia1, M., Prasad l., Bhoj C., Mathpal, C. A study of geomagnetic storms and solar and Interplanetary parameters for solar cycles 22 and 24. Solar Phys, 293:126 https://doi.org/10.1007/s11207-018-1345-y, 2008.

[2]Schwenn, R. Space weather: The solar perspective. Living Rev. Sol . Phys. 3, 2 (2006). https;//doi.org/10.1294/Irsp-2006-2, 2006.

[3]Schrijver, C.J., Bageral, F. and Sojka, J. J. HelioPhysics V, Space Weather and society. http://www.lmsal.com/schrijver/HSS5/HSS5-2015105, 2015 .pdf.

[4]Eastwood, J. P., Biffis E., Hapgood M. A., Green L., Bisi M. M., Bentley R.D., Wicks R., Mckinell L.A., Gibbs M. and Burnett C. The Economic impact of space weather: Where do we stand? Risk Analysis, vol 37, No.2, 2017 Doi: 10.1111/risa.12765.

[5]Akala, A. O., Oyeyemi, E. O., Amaechi, P. O., Radicella, S. M., Nava, B., & Amory-Mazaudier, C. Longitudinal responses of the equatorial/low-latitude ionosphere over the

oceanic regions to geomagnetic storms of May and September 2017. *Journal of Geophysical Research: Space Physics*, *125*, e2020JA027963. https://doi.org/10.1029/2020JA027963, 2020.

[6]Mendillo, M. Storms in the ionosphere: Patterns and processes for total electron content. Rev. Geophys. **44**, RG4001 (2006). doi:10.1029/2005RG000193.

[7]Magdaleno S., Herraiz M., Altadill D. and De la Morena. Climatology Characterization of equatorial plasma bubbles using GPS data.J. Space Weather Space Clim, 7 A3 (2017). Doi: 10.1051/swsc/2016039.

[8]Ndeda O. H. and Odera P. O. Analysis of Longitudinal Advancement of the peak Total Electron Content in the African equatorial anomaly region using data from GPS Receivers and GIS stations in Kenya, Canadian centre of Sc. & Educ. Applied Phys. Research: vol. 6, No. 1; 2014. Doi: 10.5539/apr.V6n.1p.19.

[9]Adewale, A. O., Oyeyemi E. O. , Adeloye A. B. , Mitchell C. N. , Rose J. A. R. , Cilliers P. J. A study of L-band scintillations and total electron content at an Equatorial station, Lagos, Nigeria. Radio science, vol. 47, RS2011, doi:10.1029/2011RS004846, 2012.

[10]Radiciella S. Workshop on science applications of GNSS in developing countries (11- 27 April) followed by the Seminar on Development and use of Ionospheric Ne Quick Model 30th April -1st May 2012, 2012.

[11]Mukherjee S., Sarkar S., Purohit P. K. and Gwal A. K. Seasonal variation of Total Electron Content at crest of equatorial anomaly station during low solar activity conditions, Adv. Spac Res., 46, 291-295, 2010.

[12]Ya'acob, N., Abdullah, M., and Ismael, M. GPS Total Electron Content (TEC) prediction of ionosphere layer over the equatorial region, Trends in Telecommunications Technologies. http://dx.org/10.577218474, 2010.

[13]Fayose, R.S., Oladosu, O.R., Rabiu, A.B. and Grooves, K.Variation of Total Electron Content [TEC] and their Effect on GNSS over Akure, Nigeria. doi:10.5539/apr.v4n2p105. http://dx.doi.org/10.5539/apr.v4n2p105, 2012.

[14] Wang, C., Shi, C., Fan, L. and Zhang, H. Improved modeling of Global Ionospheric Total Electron content using prior information. Remote sens2018,1 0, 63 doi:10.3390/r10010063, 2018.

[15]Misra, P. and Enge, P. Global positioning system signals, measurements and performance. Ganga-Jamuna press, Lincoln,Massachusetts, USA, 2001.

[16]Pedatella, N.M., Lei, J., Larson, K.M., Forbes, J.M. Observation of the ionospheric response to the 15 December 2006 geomagnetic storm: Long duration positive storm effect. J. Geophys. Res. 114, A12313, 2009.

[17] Liu, G., H. Shen. A severe negative response of ionosphere to the intense geomagnetic storm of 17 March 2015 observed at middle and low latitude stations in China zone, Advances in Space Research, 59(9), 2301-2312, doi: 10.1016/j.asr.2017.02.021, 2017.

[18]Kashcheyev, A., Migoya-Orué, Y., Amory-Mazaudier, C., Fleury, R., Nava, B., Alazo-Cuartas, K., & Radicella, S. M. Multivariable comprehensive analysis of two great geomagnetic storms of 2015. Journal of Geophysical Research: Space Physics, 123, 5000 – 5018. https://doi.org/10.1029/2017JA024900, 2018.

[19]Rukundo, W. The ionospheric dynamics of the African sector responding to a severe geomagnetic storm; the storm of 3–5 November 2021. *Space Weather, 21*, e2022SW003219. https://doi.org/10.1029/2022SW003219, 2023.

[20]Oikonomou, C., Haralambous, H., Paul, A., et al. Investigation of the negative ionospheric response of the 8 September 2017 geomagnetic storm over the European sector, Advances in Space Research, https://doi.org/10.1016/j.asr.2022.05.035, 2022.

[21]Mishra, R. K., Adhikari, B., Chapagain, N.P., Baral, R.,Das, P.K., Klausner, V., Sharma, M. Variation of Solar Wind Parameters and Total Electron Content from Indian, Australian, Brazilian and South African Sectors during the Intense Geomagnetic Storms. https://doi.org/10.1002/essoar.10503097.1, 2020. | h

[22]Sharma, S. K., Singh, A. K., Panda, S.K., Ahmed, S. S. The effect of geomagnetic storms on the total electron content over the low latitude Saudi Arab region: a focus on St. Patrick's Day storm. Astrophys Space Sci (2020) 365:35. https://doi.org/10.1007/s10509-020-3747-1.

[23]Singh, R., & Sripathi, S. Ionospheric response to 22–23 June 2015 storm as investigated using ground-based ionosondes and GPS receivers over India. Journal of Geophysical Research: Space Physics, 122. https://doi.org/10.1002/2017JA024460, 2017.

[24]Katrina, M., Ivan, P., Emmete, L. Northern lights set to return During extreme solar storm 's 2^{nd} night-Electrical utilities said they weathered earlier conditions as persistent geomagnetic storms were expected to cause another light show in the evening skies. *The New York Times, 2024.*

[25]Gurtner, W., Estey, L. Rinex-the receiver independent exchange format-version 3.00. Astronomical Institute, University of Bern and UNAVCO, Bolulder, Colorado, 2007.

[26]Seemala, G. K. GPS-TEC Analysis Application Read Me. Institute for Scientific Research, Boston college, USA, 2011.

[27]Tariku Y. A. Patterns of gps-tec variation over low-latitude regions (African sector) during the deep solar minimum (2008 to 2009) and solar maximum (2012 to 2013) phases. Earth, Planets and Space 67(1):1–9, 2015.

[28]Horvath, I., and Essex, E. A. Vertical E× B drift velocity variations and associated low-latitude ionospheric irregularities investigated with the TOPEX and GPS satellite data. Annales Geophysicae, Vol. 21, No. 4, pp. 1017-1030, 2003.

[29]Cepni MS, Potts LV, Miima JB. High-resolution station-based diurnal ionospheric total electron content (TEC) from dual-frequency GPS observations. Space Weather 11(9):520–528, 2013.

[30]Ma X, Maruyama T, Ma G, et al. Three-dimensional ionospheric tomography using observation data of gps ground receivers and ionosonde by neural network. Journal of Geophysical Research: Space Physics 110(A5), 2005.

[31]Jin, S., Park, J., Wang, J., Choi, B. and Park, P. Electron density profiles derived from Ground-based observations. The Journal of Navigation 59(3): 395-401, 2006.

[32]Heise S, Jakowski N, Wehrenpfennig A, et al. Sounding of the topside ionosphere/ plasmasphere based on GPS measurements from champ: Initial results. Geophysical Research Letters 29(14):44–1, 2002.

[33]Jawoski, N., Mayer, C., Hoque, M. and Wilken, V. Total electron content models And their use in ionosphere monitoring. Radio science, 46(06): 1-11, 2011.

[34]Ciraolo, L., Azpilicueta, F., Brunini, C., Meza, A. and Radicella, S. M. Calibration errors on experimental slant total electron content determined by the GPS. Journal of Geodesy, 81:111-120, 2007.

[35]Kassa T, Damtie B. Ionospheric irregularities over Bahir dar, Ethiopia during Selected geomagnetic storms. Advances in Space Research 60 (1):121–129, 2017.

[36]Kenpankho, P., Watthanasangmechai, K., Supnithi, P., Tsugawa, T., & Maruyama, T. Comparison of GPS TEC measurements with IRI TEC prediction at the equatorial latitude station Chumphon, Thailand. Earth, Planets and Space, 63, 365-370, 2011.

[37]Kenpankho, P., Watthanasangmechai, K., Supnithi, P., Tsugawa, T., & Maruyama, T. Comparison of GPS TEC measurements with IRI TEC prediction at the equatorial latitude station Chumphon, Thailand. Earth, Planets and Space, 63, 365-370, 2011.

[38]Ma, G., & Maruyama, T. Derivation of TEC and estimation of instrumental biases from GEONET in Japan. Annales Geophysicae, 21(10), 2083-2093, 2003.

[39]Sardon, E. and Zarraoa, N. Estimation of total electron using GPS data: How stable are the differential satellite and receiver instrumental biases? Radioscience, vol. 32, No.5, pp. 1899-1910, 1997.

[40]Liu, J., W. Wang, A. Burns, X. Yue, S. Zhang, Y. Zhang, and C. Huang. Profiles of ionospheric storm-enhanced density during the 17 March 2015 great storm, J. Geophys. Res. Space Physics,121(1), 727-744, doi:10.1002/2015JA021832, 2016.

[41]Bartels, J., Heck, N. H. and Johnson, H. F. The three-hour-range index measuring geomagnetic activity, Terr. Magn. Atmos. Electr., 44, 411-454, 1939.

[42]Kamide Y. & Chian A. Hand Book of the Solar-Terrestrial environment. SpringerBerlin Heidelberg, New York. ISBN 978-3-540-46314-6. Doi:10.007/6104478, 2007.

[43]Kutiev I, Tsagouri I, Perrone L, et al. Solar activity impact on the earth's upper atmosphere. Journal of Space Weather and Space Climate 3:A06, 2013.

[44]Sur D, Ray S, Paul A. High and mid latitude and near subsolar point ionospheric and thermospheric responses to the solar flares and geomagnetic storms during low solar

activity periods of 2017 and 2020. Advances in Space Research, 2022.

[45]Kumar S, Singh A, Lee J. Equatorial ionospheric anomaly (EIA) and comparison with IRI model during descending phase of solar activity (2005–2009). Advances in Space Research 53(5):724–733, 2014.

[46]Singh, A., Rao, S.S., Rathore, V.S., Singh S., K., and Singh, A. K. Effect of intense solar flares on TEC variation at low-latitude station Varanasi. *J Astrophys Astron* **41**, 19 (2020). https://doi.org/10.1007/s12036-020-09637-8, 2020.

[47]Zhang, R., Liu, L., Le, H., & Chen. Equatorial ionospheric electrodynamics over Jicamarca during the 6 – 11 September 2017 space weather event. Journal of Geophysical Research: Space Physics, 124, 1292 – 1306. https:// doi.org/10.1029/2018JA026295, 2019.

[48]Fuller-Rowell, T. J., Codrescu, M. V., Moffett, R. J., & Quegan, S. Response of the thermosphere and ionosphere to geomagnetic storms. Journal of Geophysical Research, 99(A3), 3893 – 3914. https://doi.org/10.1029/93JA02015. 1994.

[49]Chinmaya, N., Tsai, L. C., Su, S. Y., & Galkin, I. A. Peculiar features of the low-latitude and mid-latitude ionospheric response to the St. Patrick's Day geomagnetic storm of 17 March 2015. Journal of Geophysical Research: Space Physics, 121 (8), 7941-7960, 2016.

[50]Reddybattula, K. D., Panda, S. K., Ansari, K., & Peddi, V. S. R. Analysis of ionospheric TEC from GPS, GIM and global ionosphere models during moderate, strong, and extreme geomagnetic storms over Indian region. Acta Astronautica, 161, 283-292, 2019.

[51]Richmond, A.D., Matsushita, S. Thermospheric response to a magnetic substorm. Journal of Geophysical Research, 80, 2839–2850, 1975.

[52]Mayr, H.G., Volland, H. Magnetic Storm Characteristics of the Thermosphere. Journal of Geophysical Research, 78(13), 2251–2264, 1973.

[53]Klimenko, M. V., Klimenko, V. V. Disturbance dynamo, prompt penetration electric field and overshielding in the Earth's ionosphere during geomagnetic storm. Journal of Atmospheric and Solar-Terrestrial Physics, Vol. 90-91, pg. 145-155, doi: https://doi.org/10.1016/j.jastp.2012.02.018, 2012.

[54]Pudovkin, M.I. Electric fields and currents in the ionosphere. Space Science Reviews, 16, 727–770, 1974.

[55]Lyatsky, W.B. Current systems of magnetospheric-ionospheric disturbances. Nauka, Leningrad (in Russian), 1978.

[56]Feldstein, Ya. I. Substorm Current Systems and Auroral Dynamics. In: Magnerospheric Substorms. Kan, J.K., Potemra, T.A., Kokubun, S., lijima, T. (Eds.), American Geophysical Union, 29–41, 1991.

[57]Denisenko, V.V., Erkaev, N.V., Kitaev, A.V., Mezentsev, A.V. Mathematical modeling of the magnetospheric processes, Nauka, Novosibirsk (in Russian), 1992.

[58]Ponomarev, E.A., Sedykh, P.A. How can we solve the problem of substorms? (A review). Geomagnetism and Aeronomy, 46(4), 530–544, 2006.

[59]Blanc, M., & Richmond, A. The ionospheric disturbance dynamo. *Journal of Geophysical Research, 85,* 1669–1686. https://doi.org/10.1029/ja085ia04p01669, 1980.

[60]Mazaudier, C., R. Bernard, and S. V. Venkateswaran. Correction to "Saint-Santin radar observations of lower thermospheric storms", J. Geophys. Res., 90, 6685 – 6686, doi:10.1029/JA090iA07p06685, 1985.

[61]Fejer, B. G., Larsen, M. F., & Farley, D. T. Equatorial disturbance dynamo electric fields. Geophysical Research Letters, 10(7), 537 – 540. https://doi.org/10.1029/GL010i007p00537, 1983.

[62]Fejer, B. G. Equatorial ionospheric electric fields associated with magnetospheric disturbances in solar wind magnetospheric coupling. In Y. Kamid & J. A. Salvin (Eds.), Solar wind-magnetosphere coupling, Terra Sci. Tokyo (pp. 510 – 545). Dordrecht, Holland: D. Reidel, 1986.

[63]Sastri, J. H., Ramesh, K. B., & Rangnath Rao, H. N. C. Transient composite electric field disturbances near dip equator with auroral substorms. Geophysical Research Letters, 19(14), 1451 – 1454. https://doi.org/10.1029/92GL01447, 1992.